Journal of Materials Chemistry B

Accepted Manuscript

ROYAL SOCIETY OF CHEMISTRY

www.rsc.org/materialsB

Journal of Materials Chemistry B

RSCPublishing

ARTICLE

Dual-core@shell-structured Fe_3O_4-$NaYF_4$@TiO_2 Nanocomposites as Magnetic Targeting Drug Carrier for Bioimaging and Combined Chemo-sonodynamic Therapy

Cite this: DOI: 10.1039/x0xx00000x

Received 00th January 2012,
Accepted 00th January 2012

DOI: 10.1039/x0xx00000x

www.rsc.org/

Song Shen [ab], Xiaomeng Guo [b], Lin Wu [c], Meng Wang [b], Xinshi Wang [b], Fenfen Kong [b], Haijun Shen [b], Meng Xie [b], Yanru Ge[*] [a] and Yi Jin[*] [b]

Multifunctional dual-core@shell (Fe_3O_4-$NaYF_4$@TiO_2) nanocomposites (DCSNCs) loaded doxorubicin (DOX) have been developed for synergetic sonodynamic cancer chemotherapy, where titanium dioxide (TiO_2) is employed as a sonosensitizer for sonodynamic therapy (SDT) of the tumor in deep tissue, and $NaYF_4$ is used for upconversion luminescence (UCL) imaging. After being coated with hyaluronic acid (HA), the nanocomposites exhibit time dependent cellular uptake and excellent nucleus targeting effect in KB and MCF-7 cells. The ultrasound of HA-DCSNCs obviously enhances the apoptosis rate of MCF-7 cells. Greater tumor inhibition rate is observed when the tumor-bearing mice are treated with combined therapy (88.36%) compared with chemotherapy (28.36%) or sonodynamic therapy (38.91%) alone, indicating the potential of sonodynamic chemotherapy for cancer treatment.

1. Introduction

Sonodynamic therapy (SDT) employs sonosensitizers to generate reactive oxygen species (ROS) by the activation of ultrasound (US), leading to the destruction of cancer cells. [1-3] As an approach derived from photodynamic therapy (PDT), SDT overcomes the limitation of poor light penetrability [2, 4, 5] and is expected to be an effective therapeutic tool for the tumors developed in deep tissue due to appropriate tissue attenuation coefficient of US. Various sonosensitizers such as 5-aminolevulinic acid, [6, 7] ATX-70 [1, 8] and TiO_2 [2, 3] have been developed for SDT treatment of cancers. Among these, TiO_2 has attracted considerable interest in biological applications [9, 10] due to its fascinating features such as low toxicity, good biocompatibility and high stability in physiological environment [11, 12]. However, for potential use of SDT in the clinic, better tumor targeting and therputic monitoring in vivo are required to improve treatment efficacy and reduce side effects. Besides, monotherapy becomes powerless in cancer therapy for the multidrug resistance (MDR). It is, therefore, critical to develop multifunctional nanoparticles (NPs) with integrated functions such as combined therapy, favorable tumor-targeting ability and tumor diagnosis.

Lanthanide-doped upconversion nanophosphors (UCNPs), which can be excited by near-infrared (NIR) (900-1000 nm) continuous-wave (CW) laser light to give emission in the visible region, have shown promising applications in bioimaging. [13-15] As alternatives to traditional fluorescent probes such as quantum dots (QDs) [16, 17] and organic dyes, [18, 19] UCNPs have attractive chemical and optical features, including large stokes shifts, low toxicity, good photostability and weak autofluorescence backgrounds, etc. [20-22] To improve tumor targeting efficiency, UCNPs can be further functionalized with magnetic iron oxide (Fe_3O_4) nanoparticles (IONPs). Presently, a number of multifunctional paltforms based on UCNPs and IONPs have been developed. [15, 23-25] However, few multifunctional platforms that using TiO_2 as shell and simultaneously for chemotherapy and SDT have been reported for the difficulty to control the hydrolysis of tetrabutyl titanate (TBOT).

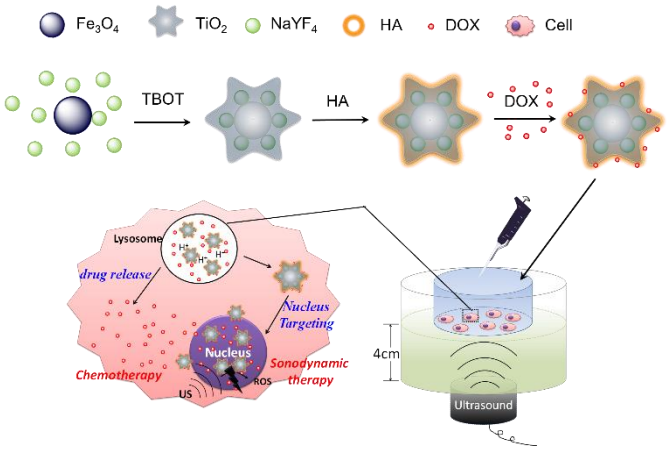

Scheme 1. Schematic diagram illustrating the synthesis of HA coated Fe_3O_4-$NaYF_4$@TiO_2 nanocomposites (HA-DCSNCs) and the concept of combined sonodynamic chemotherapy.

Herein, a multifucntional platform of dual-core@shell nanocomposites (DCSNCs) with $NaYF_4$-based UCNPs and magnetic Fe_3O_4 nanoparticles as cores and TiO_2 as shell has been fabricated via the Stober method (Scheme 1). In this nanocomposites, TiO_2

possesses multi-functions including sonodynamic therapy, nucleus targeting and chemotherapy drug loading. The results of in vivo experiments demonstrated the outstanding UC luminescence (UCL) imaging ability, good tumor targeting effect, and excellent synergistic therapeutic efficacy of the fabricated nanocomposites. These results may indicated the potential of HA-DCSNCs for combined sonodynamic chemotherapy in cancer treatment.

2. Experiment and methods

2.1 Materials

Iron (III) chloride hexahydrate ($FeCl_3$ $6H_2O$), ethylene glycol (EG), anhydrous ethanol, trisodium citrate dehydrate, sodium acetate trihydrate (NaAc $3H_2O$), tetrabutyl titanate (TBOT) and concentrated ammonia solution (28 wt%) were purchased from Sinopharm Chemical Reagents Company. Hoechst 33342, propidium iodide (PI) were obtained from Sigma-Aldrich. Annexin V-FITC/PI apoptosis detection kit was purchased from Beyotime Co., Ltd. (China). Ytterbium nitrate pentahydrate ($Yb(NO_3)_3$ $5H_2O$), yttrium nitrate hexahydrate (YNO_3 $6H_2O$) and erbium trinitrate pentahydrate ($ErNO_3$ $5H_2O$), branched polyethylenimine (PEI, 10 kDa) and Hyaluronic acid sodium salt (HA) were purchased from Aladdin Reagent Co., Ltd. (China). Doxorubicin hydrochloride (DOX) was purchased from Dalian Meilun Biology Technology Co. Ltd. (Dalian, China). All chemicals were used without further purification. Deionized water (18.4 MΩ cm) used in all experiments was prepared by Milli-Q system (Millipore, USA).

2.2 Measurements and characterizations

Morphology and structure of the prepared Fe_3O_4, $NaYF_4$ and DCSNCs particles were characterized on a JEM-2100 F transmission electron microscope at an accelerating voltage of 200 kV. Powder X-ray diffraction (XRD) patterns were recorded on an X'Pert Pro (Panalytical, The Netherland s) diffraction meter with Cu Kα radiation at $\lambda = 0.154$ nm operating at 40 kV and 40 mA. Size distribution of the particles was measured on a Malvern Zetasizer Nano ZS90 instrument at room temperature. Thermal gravimetric analysis (TGA) analysis was performed on a thermogravimetric analyzer (NETZSCH TG209) under nitrogen atmosphere. Upconversion fluorescence spectra were obtained on a luminescence spectrometer (RF-5301PC, Shimadzu) with an external 980 nm semiconductor lasers (Wuhan ZJKC Technology Co., Ltd.) as the excitation source. A Maestro imaging system (CRI, Inc., Woburn, MA) equipped with 980 nm lasers was used to perform phantom imaging and in vivo mouse imaging. The US apparatus was the commercially available (838A-H-O-S, Shengxiang ultrasonic, China). In vivo experiments were performed in compliance with Zhejiang University Animal Study Committee's requirements for the care and use of laboratory animals in research.

2.3 Synthesis of HA coated Fe_3O_4-$NaYF_4$@TiO_2 dual-core@ shell nanocomposites (HA-DCSNCs)

2.3.1 Synthesis of $NaYF_4$: Yb, Er Nanoparticles

In a typical synthesis procedure, $Yb(NO_3)_3$ (0.54 mmol), $Y(NO_3)_3$ (2.4 mmol), $Er(NO_3)_3$ (0.06 mmol), and NaCl (6 mmol) were dissolved in 40 mL of EG. Under vigorous stirring, another EG solution (30 mL) containing PEI (0.75 g) and NH_4F (0.888 g) was added. The resulting mixture was agitated for another 30 min, then transferred to a 80 mL of Teflon-lined autoclave, and subsequently heated at 200 ℃. After 8h hydrothermal treatment, the autoclave was cooled down to room temperature in air. Then the nanoparticles were obtained by centrifugation, washed with ethanol and DI water for several times, and preserved in ethanol for further use.

2.3.2 Synthesis of Magnetic Particles

The Fe_3O_4 particles were synthesized using a modified solvothermal reaction.[26, 27] Typically, $FeCl_3$ $6H_2O$ (1.62 g, 6 mmol) and trisodium citrate dihydrate (0.60 g, 2.04 mmol) were dissolved in ethylene glycol (60 mL) to form a clear solution. With the addition of NaAc (3.6 g), the mixture was stirred vigorously for 1 h and then transferred into teflon-lined stainless-steel autoclave (80 mL capacity). Hydrothermal reactions were conducted at 200 ℃ for 12 h. After hydrothermal reaction, the black sample was collected with the help of an external magnetic field and then rinsed with alcohol and distilled water for several times. The final Fe_3O_4 particles were obtained and preserved in water for further use.

2.3.3 Synthesis of DCSNCs

The Fe_3O_4-$NaYF_4$@TiO_2 nanocomposites were synthesized by directly coating a TiO_2 layer on the composite of Fe_3O_4 and $NaYF_4$ in the mixed solvent of ethanol and acetonitrile at room temperature via sol−gel process of hydrolysis and condensation of TBOT. Briefly, about 10 mg of Fe_3O_4, 60 mg of $NaYF_4$ and 0.5 mL of NH_3 H_2O were added to a mixed solvent containing 90 mL of ethanol and 30 mL of acetonitrile and insonated for 10 min to disperse the particles. Then, 0.5 mL of TBOT was added to the above suspension under ultrasound. After insonating for 1.5 h, the products were collected by magnetic separation and washed with ethanol for several times.

2.3.4 HA coating on DCSNCs

Coating of HA on DCSNCs was carried out following a literature protocol. [28] DCSNCs (50 mg) was dispersed in 10 mL water following by sonication for 10 min. 10 ml HA solution (10 mg mL^{-1}) was added slowly into the DCSNCs dispersion. After stirring for 12h, the HA coated DCSNCs (HA-DCSNCs) were collected with the help of a permanent magnet. The resulted brown precipitates were washed with distilled water for two times to remove unbound HA.

2.4 Loading and releasing of doxorubicin

DOX loading onto HA-DCSNCs was done by simply mixing 10 mL HA-DCSNCs (400 μg·mL^{-1}) with 10 mL DOX solution with different concentrations of 50, 100, 150, 200, 300 μM for 24 h. Unbound DOX was removed by centrifugation and washed thoroughly with water (over 3 times) until the supernatant was colorless. The formed complexes (denoted as HA-DCSNCs-DOX) were then resuspended and stored at 4 ℃.

The pH sensitive release kinetics of DOX from HA-DCSNCs samples were determined in phosphate buffered saline (PBS, pH 5.0, 6.5 and 7.4 respectively) at 37 ℃. DOX molecules that released from the HA-DCSNCs surfaces over time were collected from supernatant by centrifugation. DOX concentrations were determined using UV–Vis spectroscopy at 483 nm. Data were expressed as mean value of three independent experiments with the reported standard deviation.

2.5 Sonodynamic therapy

To evaluate the SDT effect, MCF-7 (human breast carcinoma cell line) cells were incubated with cultrue medium (control), 100 μg·mL^{-1} HA-DCSNCs or 100 μg·mL^{-1} HA-DCSNCs-DOX (the concentration of DOX is 10 μg·mL^{-1}) for 4 h at 37 ℃. After replacing the HA-DCSNCs or HA-DCSNCs-DOX with PBS, the cells were treated with ultrasound at the intensity of 1 W cm^{-2} for 0 min, 0.5 min,

1 min, 3 min, 5 min respectivley. Then the treated cells were incubated for another 12 h in cultrue medium for further determination.

2.6 Cytotoxicity and sonodynamic therapy (SDT) evaluation

To determine the cytotoxicity of HA-DCSNCs, MCF-7 (5×10^3) cells were seeded onto 96-well plates and incubated for 24 h. Then 25 μL of HA-DCSNCs dispersed in culture medium with various concentrations were added to each well. After incubated for another 24 h, the cell viability was determined using 3-(4,5-dimethylthiazol-2-yl)-2,5-diphenyltetrazolium bromide (MTT) method. SDT induced cell damage in the presence of HA-DCSNCs or HA-DCSNCs-DOX was detected using the MTT method.

2.7 Cell uptake

To investigate the intracellular kinetics and distribution of HA-DCSNCs, KB (human oral squamous carcinoma cell line) and MCF-7 cells (1×10^5) were cultured onto 20-mm glass coverslips for 24 h. Then the medium was replaced with 1 mL of fresh culture medium containing 50 μg HA-DCSNCs-DOX. After incubation for 1, 2 and 4 h, the cells were rinsed three times with PBS and then stained with hoechst 33342. The cellular fluorescence images were examined under a Zeiss LSM710 two-photon confocal microscopy. The UC luminescent signals (600–700 nm) were collected.

2.8 Flow cytometry analysis

In the flow cytometry analysis, cells were randomly divided into six groups: control group, US group, HA-DCSNCs group, US + HA-DCSNCs group, HA-DCSNCs-DOX group and US + HA-DCSNCs-DOX group. After the incubation with cultrue medium (control), HA-DCSNCs (100 $\mu g\cdot mL^{-1}$) or HA-DCSNCs-DOX (100 $\mu g\cdot mL^{-1}$) (the concentration of DOX was 10 $\mu g\cdot mL^{-1}$) for 4 h at 37 ℃, the HA-DCSNCs or HA-DCSNCs-DOX was replaced with PBS. Then the cells were insonated in the dark for 3 min at the intensity of 1 W cm^{-2} and incubated for another 12 h. The apoptosis and necrosis of MCF-7 cells were determined using an Annexin V-FITC apoptosis kit by flow cytometry.

2.9 Detection of reactive oxygen species (ROS)

The intracellular ROS generation was determined using the probe 2, 7-dichlo-rofluorescein (DCF). After incubated with or without DCSNCs (100 $\mu g\cdot mL^{-1}$) for 4 h, the cells were then incubated with 10 μM 2'-7'-dichlorofluorescin diacetate (DCFH-DA) for 30 min. Then the cells were treated with US for 3 min and stained with hochest 33342. The cellular fluorescence images were examined under a Zeiss LSM710 confocal microscope.

2.10 In vivo UCL imaging

ICR mice were obtained from Shanghai Laboratory animal center and used under protocols approved by Zhejiang University Laboratory Animal Center. To develop tumor bearing mice, S180 cells (1×10^7 cells) were implanted subcutaneously into the shoulder of each mouse. Then, 200 μL of HA-DCSNCs solution (10 $mg\cdot mL^{-1}$) was intravenously injected to the mice when the tumor reached approximately 100 mm^3. To study the magnetic targeting effect, a small magnet was attached onto the tumor for 24 h while other mice without magnet were used as control. Then the tumor-bearing mouse was taken for UCL imaging using the Maestro in vivo imaging system (CRi Inc.) with an external 980 nm laser (1.5 W cm^{-2}) as the excitation source. An 850 nm short-pass filter was fixed before the CCD camera to exclude the excitation light. The UCL signals at 640-680 nm from HA-DCSNCs were collected. At the end of the experiments, the animals were euthanized according to standard approved protocol.

2.11 Biodistribution of HA-DCSNCs-DOX

For fluorescence imaging, 200 μL of free DOX or HA-DCSNCs-DOX was intravenously injected into S180 tumor bearing mice for in vivo imaging. At defined time points (2, 6, 12, 24 and 48 h after injection), the mice were killed, and the organs (heart, lung, spleen, liver, kidney, tumor) were harvested and imaged using the Maestro in vivo imaging system.

2.12 Combined sonodynamic chemotherapy in vivo

S180 cells (1×10^7 cells) were implanted subcutaneously into the mice to develop tumor bearing mice. Several mice with two tumors were also developed.Several mice with two tumors were also developed. When the tumor reached approximately 100 mm^3, the mice with one tumor were divided into three groups (n = 5 per group) to receive normal saline (200 μL), saline (200 μL) + ultrasound, or free DOX (200 μL, 3 $mg\cdot kg^{-1}$). The mice with two tumors were injected with equivalent dose of HA-DCSNCs-DOX (200 μL, 3 $mg\cdot kg^{-1}$). After intravenous injection and under tumor magnetically targeted field for 24 h, the tumors were exposed to ultrasound at the power intensity of 1 W cm^{-2} for 3 min. The above treatment was carried out every 3 days and repeated for 4 times. The tumor sizes were measured by a caliper every other day and calculated as the volume=(tumor length) ×(tumor width) $^2/2$.

3. Results and Discussion

3.1 Preparation and Characterization of HA-DCSNCs

IONPs were synthesized by a reduction reaction between $FeCl_3$ and ethylene glycol in the presence of trisodium citrate (Na_3Cit). [26, 27] Transmission electronic microscopy (TEM) images revealed that the IONPs were monodispersed spherical nanocrystals with average diameters of approximately 150 nm (Figure 1 a, Supporting Information Figure S1). Monodispersed cubic $NaYF_4$-based UCNPs (Y/Yb/Er = 78:20:2) with an average diameter of about 50 nm were synthesized according to literature protocols using polyethylenimine (PEI) as stabilizer [14] (Figure 1d, Supporting Information Figure S1).

The protocol for the synthesis of the Fe_3O_4-$NaYF_4$@TiO_2 nanocomposites is illustrated in Scheme 1. Typically, the obtained Fe_3O_4 NPs and $NaYF_4$ NPs were dispersed in ethanol/acetonitrile mixtures by ultrasound for 10 min. The negatively charged carboxyl groups provided by the citrate stabilizer endowed the IONPs outstanding dispersibility and also adsorbed positive amidogen, which drew the IONPs and PEI modified $NaYF_4$ NPs together. Then, uniform dual-core@shell Fe_3O_4-$NaYF_4$@TiO_2 nanocomposites were obtained via sol−gel process of rapid hydrolysis and condensation of TBOT. [29, 30] Representative TEM images revealed the dual-core@shell structure of the composites (Figure 1b, c). The presence of IONPs and UCNPs in one particle was also confirmed by the combined results of compositional analysis (Figure 1e) and energy-dispersive X-ray (EDX) elemental maps (Figure 1g) of an individual Fe_3O_4-$NaYF_4$@TiO_2 particle. To improve the tumor targeting effect, the as-prepared DCSNCs were then functionalized with hyaluronic acid by physical absorption. [28] According to the TG analysis (see Supporting Information, Figure S2), the hyaluronic acid accounts was 1.7 wt. % of the composites. The obtained DCSNCs could disperse well in water and showed greenish upconversion light (UCL) emission with the irradiation of 980 nm laser light (Figure 1f). The

zeta potentials of the DCSNCs and HA-DCSNCs NPs were -24.6 mV and -35.4 mV.

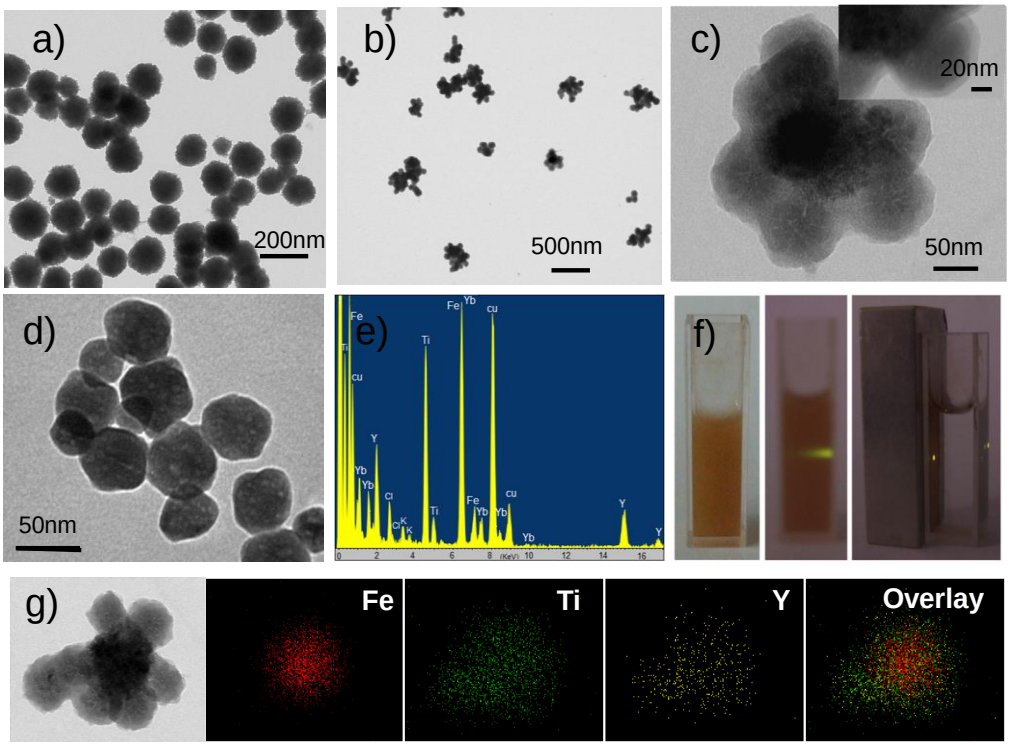

Figure 1. Characterization of the $NaYF_4$, Fe_3O_4 and DCSNCs. TEM images of the a) Fe_3O_4; b, c) as prepared DCSNCs; d) $NaYF_4$. e) EDX spectrum of the DCSNCs. f) Photos of the DCSNCs aqueous solution (1 mg mL^{-1}) under ambient light (left), exposed to a 980 nm laser (middle), and with a magnetic field (right). g) TEM and EDX maps of the distribution of Fe, Ti, and Y elements in DCSNCs.

3.2 Drug loading and releasing on HA-DCSNCs

The doxorubicin (DOX) loading and releasing behaviors of HA-DCSNCs were then studied. To determine the saturated loading capacity of DOX on HA-DCSNCs, the HA-DCSNCs solutions (0.2 mg mL^{-1}) were mixed with different concentrations of DOX in water for 24 h at room temperature and then washed thoroughly to remove unbound DOX. When the DOX concentration reached 200 μM, a maximal DOX loading capacity of 15.7% (w/w) was observed (Figure 2a). The color of the HA-DCSNCs changed from yellowish to henna due to the adsorption of DOX (Supporting Information Figure S3). HA-DCSNCs-DOX displayed a characteristic DOX absorption peak at ~490 nm (Figure 2b). In terms of release, the total amount of DOX released from the HA-DCSNCs increased under acidic conditions (47.9% (w/w) at pH 7.4, 51.5% (w/w) at pH 6.5, and 59.1% (w/w) at pH 5.0, respectively) (Figure 2c). This trend was attributed to the increased hydrophilicity and higher solubility of DOX at lower pH, which reduced the electrostatic interaction between DOX and HA-DCSNCs. [31] The pH-sensitve drug release was expected to minimize premature release of the cytotoxic drug during blood circulation and facilitate the active drug release at the acid target issues such as the microenvironments of extracellular tissues of tumors and intracellular lysosomes and endosomes. [32] The UCL spectra of UCNPs, HA-DCSNCs and HA-DCSNCs-DOX were also measured using a 980 nm laser as the excitation light (Figure 2d). Compared with the spectrum of UCNPs, an obvious decrease of the UCL emission band from 510 to 560 nm (green band) was found in HA-DCSNCs, which was attributed to the quenching effect [33, 34] and adsorption of Fe_3O_4 (Supporting Information, Figure S4). Then the green emission was further quenched after the loading of DOX due to the selective energy transfer from UCNPs to DOX, while the 650 nm band was not. This could be visualized from the obvious green fluorescence quench of the HA-DCSNCs-DOX, as given in Figure 2d inset. Although the energy was transfered from UCNPs to DOX, no emission of DOX observed. This phenomenon perhaps is due to the weak energe of excitation light.

Journal of Materials Chemistry B RSCPublishing

ARTICLE

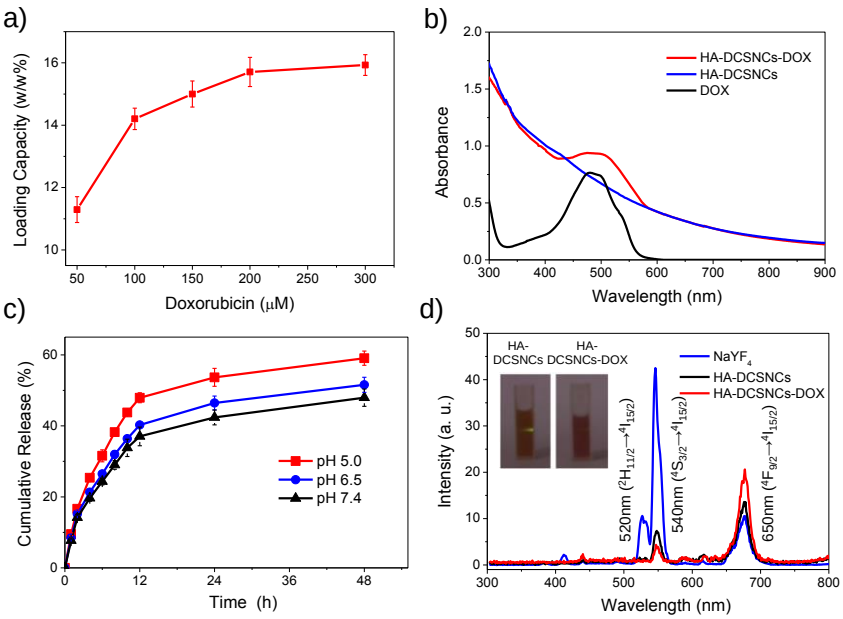

Figure 2. Loading and releasing of DOX in the HA-DCSNCs. a) Quantification of DOX loading at different DOX concentrations (in water). b) UV-vis absorbance spectra of free DOX, bare HA-DCSNCs, and HA-DCSNCs-DOX solutions. c) DOX release profiles from HA-DCSNCs-DOX conjugates at pH 5.0, pH 6.5 and pH 7.4. d) Room temperature UCL spectra of $NaYF_4$, HA-DCSNCs and HA-DCSNCs-DOX, inset: UCL photographs of HA-DCSNCs and HA-DCSNCs-DOX.

3.3 Sonodynamic therapy in vitro

The cytotoxity of HA-DCSNCs was investigated on the MCF-7 cells using the 3-(4, 5-dimethylthiazol-2-yl)-2, 5-diphenyltetrazolium bromide (MTT) assay. As shown in Figure 3a, HA-DCSNCs had little influence on MCF-7 cells during 24 h incubation. Cell viability was over 85% when the concentration of HA-DCSNCs was 1000 μg·mL^{-1}. To access the anticancer effect of SDT, we studied the cytotoxicity of HA-DCSNCs and HA-DCSNCs-DOX upon the irradiation of US using PBS as control at the intensity of 1 W cm^{-2} for different time. The irradiation of US exhibited significantly enhanced cytotoxicity both in HA-DCSNCs and HA-DCSNCs-DOX treated cells, while no obvious influence in PBS group (Fig. 3b). Besides, the cytotoxicity increased as the US time extended. The MTT assays of cell viability were further confirmed by microscopic observations. As shown in Figure S5, MCF-7 cells became increasingly round and nonadherent with the increasement of irradiation time, while no obvious change in cellular morphology was observed in the absence of US irradiation.

3.4 Cellular uptake

To investigate the intracellular behavior, HA-DCSNCs-DOX were coincubated with KB (human oral squamous carcinoma cell line) and MCF-7 (human breast carcinoma cell line) cells at the concentration of 50 μg·mL^{-1} and imaged using two-photon confocal microscope. The cellular uptake and subsequent localization of HA-DCSNCs-DOX after 1, 2, and 4 h incubations were shown in Figure 3c and Supporting Information, Figure S6. It could be seen from the figures that the HA-DCSNCs-DOX had excellent time-dependent cellular uptake ability. More importantly, HA-DCSNCs showed obvious nuclear affinity and could deposit in nucleus, which indicated the potential for nucleus targeting drug delivery. As we know, the action mechanism of DOX is to intercalate DNA and RNA in the nucleus. So the HA-DCSNCs-mediated nucleus localization would increase the antitumor efficacy of DOX.

3.5 Flow cytometry analysis

To investigate the apoptosis induction effect of HA-DCSNCs and HA-DCSNCs-DOX, MCF-7 cells were labeled with Annexin V-FITC (fluoresceine isothiocyanate) and PI (propidium iodide) before analysis by flow cytometry. As shown in Figure 3d, no significant difference in early apoptosis of HA-DCSNCs (1.54%) or US (1.78%) treated MCF-7 cells was found compared with control cells (1.3%), while the percentage of apoptotic cells dramatically increased to 15.15% after the treatment of HA-DCSNCs-mediated SDT under the intensity of 1 W cm^{-2} for 3 min. These findings demonstrated that sonodynamic activation of HA-DCSNCs could induce the early apoptosis of MCF-7 cells effectively. Many late apoptotic cells and necrosis cells were observed when the cells treated with HA-DCSNCs-DOX alone, indicating the strong cytotoxicity of DOX. Upon US irradiation, HA-DCSNCs-DOX treated MCF-7 cells showed a further increase in late apoptotic cells and necrosis cells. The above results suggested that US would augment the toxicity of DOX and accelerate the apoptosis and necrosis of MCF-7 cells.

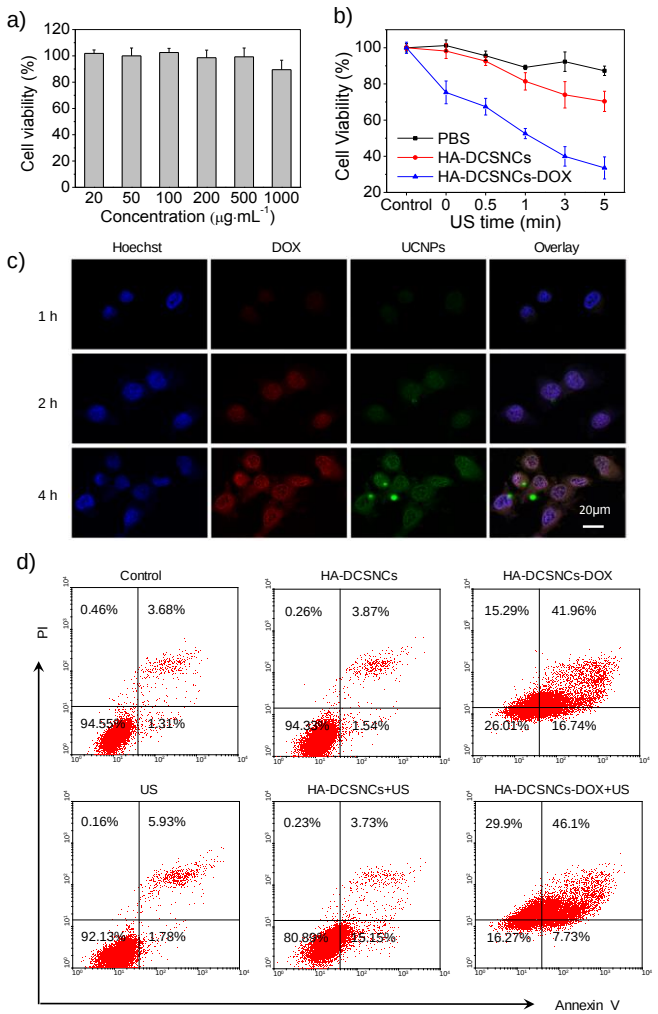

Figure 3. Evaluation of HA-DCSNCs and HA-DCSNCs –DOX in KB and MCF-7 cells. a) Cell viability curves of MCF-7 cells incubated with different concentrations of HA-DCSNCs for 24 h. b) Cell viability after incubated with HA-DCSNCs (100 μg mL^{-1}) and US at intensities of 1.0 W cm^{-2} for 0.5 min, 1 min, 3 min and 5 min. c) Uptake of HA-DCSNCs-DOX in KB cells with different incubation time. d) Apoptosis and necrosis ratio of MCF-7 cells after different treatments analyzed using flow cytometry with Annexin V-FITC and PI staining.

3.6 ROS generation

Next, we attempted to explore the mechanism underlying SDT. The intracellular generation of ROS which was widely considered as an active ingredient in SDT was determined by measuring conversion of nonfluorescent DCFH-DA to fluorescent DCF. DCF fluorescence was imaged by fluorescence microscopy with the same exposure time. As shown in Supporting Information, Figure 4a, no fluorescence could be seen in most of control cells. When the cells were treated with HA-DCSNCs+US, bright green fluorescence of DCF emerged, in marked contrast to the extremely weak fluorescence in HA-DCSNCs or US treated cells. Coincubation with NAC significantly attenuated the fluorescence of DCF, further suggesting the generation of ROS during SDT. The intracellular localization of ROS was then studied by staining the cells with hoechst 33342 (Figure 4b). In the cells treated with HA-DCSNCs+US, the green fluorescence appeared and was completely overlapped with the location of HA-DCSNCs, indicating the ROS was generated by the irradiation of HA-DCSNCs. The green fluorescence of DCF was also found in US treated cells, however the fluorescence was weak and mainly located out of the nucleus. The above results indicate the favorable nucleus targeting ability of HA-DCSNCs and the potential of using as sonosensitizer.

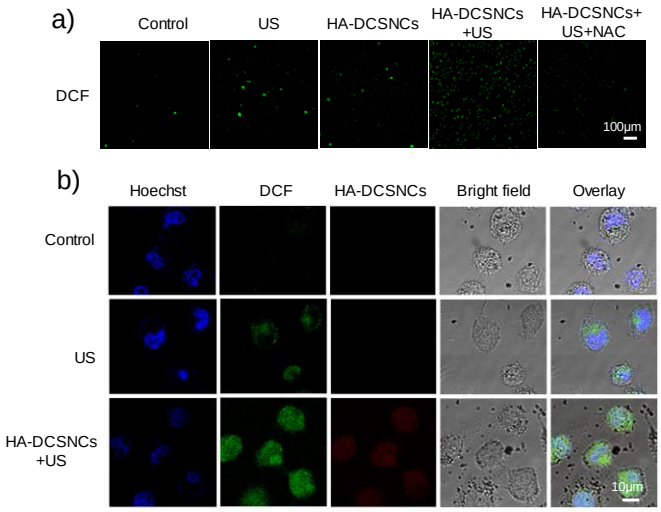

Figure 4. Fluorescent photomicrograph of MCF-7 cells stained by DCFH-DA showing intracellular ROS. a) with low magnification. b) with high magnification.

3.7 In vivo UCL imaging and biodistribution of HA-DCSNCs

The in vivo imaging and magnetic tumor targeting effect of HA-DCSNCs were evaluated by the Maestro in vivo imaging system (CRi Inc.) equipped with a 980 nm laser (1.5 W cm^{-2}). After intravenous injection with HA-DCSNCs (200 μL of 10 mg·mL^{-1}), S180 tumors-bearing mice with or without magnetic targeting were taken for in vivo imaging. As shown in Figure 5a, bright UCL signal was observed both from the tumors with and without external magnetic field (MF). However, the UCL signal was much brighter in the tumor treated with MF. The above results indicated the excellent magnetic tumor targeting effect of the HA-DCSNCs, which could be applied as luminescent imaging probe for tumor diagnosis and targeting drug delivery.

HA-DCSNCs are expected to transfer anticancer drug to tumor and decrease the location in normal tissues. So the biodistribution of DOX loaded HA-DCSNCs was investigated with free DOX as control. After intravenous injection with free DOX (3 mg kg^{-1}) and equivalent dose of HA-DCSNCs-DOX, the mice were sacrificed at certain time points (2, 6, 12, 24 and 48 h post injection). Then, the major organs were harvested and imaged by the in vivo imaging system. Figure 5b shows time-dependent fluorescent images of the major organs. It is quite evident that mice injected with HA-DCSNCs-DOX showed a liver accumulation over a period of 12 h, which might be attributed to the capture of HA-DCSNCs-DOX by the reticule endothelial system (RES). The maximum fluorescence was acquired from the tumor 24 h post injection, indicating the obvious accumulation of HA-DCSNCs-DOX in tumor. In contrast, free DOX was quickly distributed in the liver, kidney and tumor at the initial of injection. 24 h later, the DOX in the tumor was significantly lower than that injected with HA-DCSNCs-DOX (shown in Figure 5c). A quantitative assessment of the biodistribution at 12 h showed a strong fluorescence in kidney demonstrating the quick excretion of free DOX (Supporting Information, Figure S7). In the biodistribution profile of 48 h, bright

fluorescence was observed in the tumor treated with HA-DCSNCs-DOX, which was 2.5 times higher than that of free DOX (Supporting Information, Figure S8), indicating the significant tumor targeting effect and long lasting location of HA-DCSNCs-DOX also the great potential of HA-DCSNCs-DOX for cancer therapy. We can also see the obvious decrease of fluorescent signal of HA-DCSNCs-Dox in liver in 48h. This phenomenon is possibly due to the release of DOX from HA-DCSNCs and thus quick metabolism and elimination from the body.

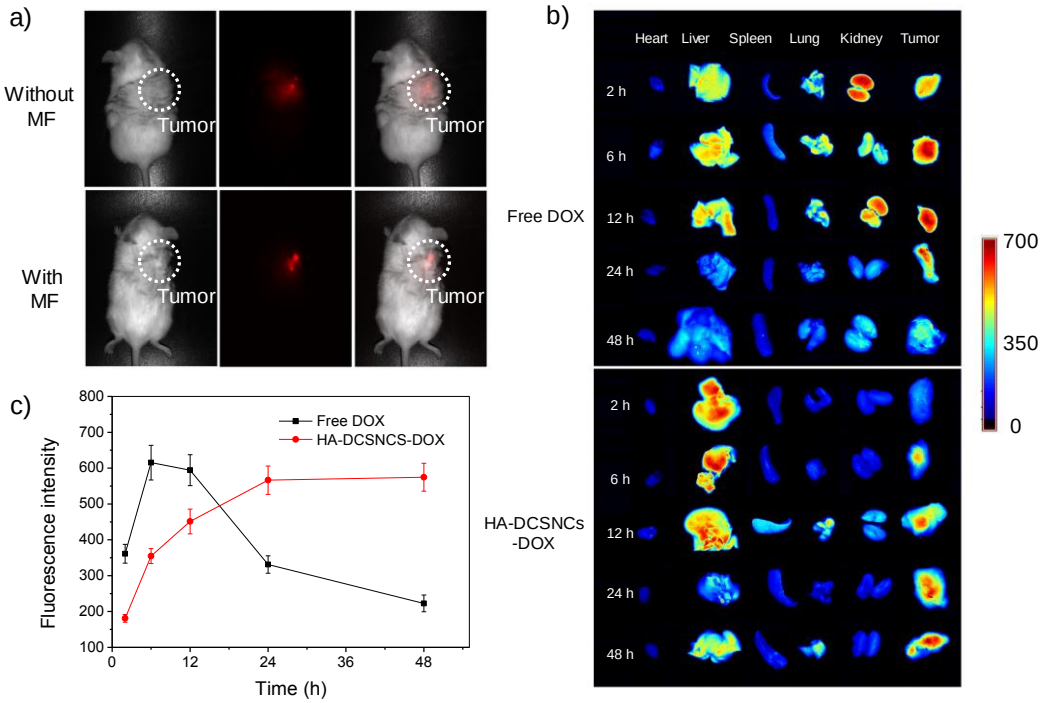

Figure 5. In vivo imaging and biodistribution of HA-DCSNCs. a) In vivo UCL images of HA-DCSNCs injected ICR mice in bright field (left), dark field (middle), and overlay (right) under magnetic field (below) and without magnetic field (above). b) Fluorescence images showing the ex vivo biodistribution of DOX and HA-DCSNCs-DOX after intravenous injection. c) Fluorescence intensity of DOX in tumors at different time points post the injection of free DOX and HA-DCSNCs-DOX respectively.

3.8 Combined sonodynamic chemotherapy in vivo

Considering the remarkable tumor targeting effect, the in vivo combined sonodynamic and chemotherapy experiment was further conducted in ICR mice. As we known, KB and MCF-7 which are human cell lines can not be used to develop tumors in ICR mice. So transplant subcutaneous model of sarcoma S180 was constructed. The tumors bearing mice were randomly divided into five groups: saline, saline+US, free DOX, HA-DCSNCs-DOX, HA-DCSNCs-DOX+US. After intravenous injection and magnetic targeting for 24 h, the tumors with and without US irradiation were monitored by measuring the tumor volume every other day. As shown in Figure 6a, the growth of tumor treated with US, free DOX and HA-DCSNCs-DOX was inhibited. However, the tumor inhibition rate was only 38.91 %, 28.36 % and 26.91 % respectively. Besides, no significant difference in tumor growth inhibition between HA-DCSNCs-DOX and free DOX group was found, although better tumor targeting effect was observed in HA-DCSNCs-DOX group (Figure 5b, c). Perhaps, the emergence of multidrug resistance (MDR) should be responsible for this phenomenon. In the mice treated with HA-DCSNCs-DOX+US, tumor growth was effectively suppressed (also confirmed by digital photos in Figure 6b, c), indicating the synergistic therapeutic effect offered by the combination therapy. Significant difference in tumor mass was observed compared with other four groups (saline, saline+US, free DOX, HA-DCSNCs-DOX), $P<0.001$ (Figure 6d). Therapeutic effect of HA-DCSNCs-DOX was confirmed by histological examination (Figure 6e). Marked degenerative changes of coagulative necrosis, including karyorrhectic debris and considerable karyolysis, were found in saline+US, free DOX, HA-DCSNCs-DOX and HA-DCSNCs-DOX+US groups. What's more, almost all of tumor cells were severely destroyed in the group receiving both HA-DCSNCs-DOX injection and US irradiation. These results were in good agreement with the tumor growth data, further confirming the superior therapeutic efficacy of the combined cancer therapy using HA-DCSNCs-DOX. The influence of HA-DCSNCs-DOX on other organs of mice was also investigated. Compared with the control group, no noticeable sign of organ damage or inflammatory lesion was observed in these major organs (Figure S9), indicating the low toxic and side effect of the HA-DCSNCs-DOX.

The synergistic antitumor effect obtained in this experiment may be ascribed to the following three reasons. Firtst, the good tumor and nucleus targeting effect of HA-DCSNCs will enhance the toxicity of DOX (Figure 3c). Second, the generation of ROS is considered as the main reason of the cancer cells damage in SDT. [35] While chemical drug such as DOX induces apoptosis of tumor cells mainly by oxidative DNA damage. [36] Therefore, it is rationally to reckon that SDT would act synergistically with chemotherapy in cancer treatment. Third, ultrasound (US) which can cause transient membrane permeability has the potential for promoting the delivery of molecules into the cytoplasm. [37]

Journal of Materials Chemistry B RSCPublishing

ARTICLE

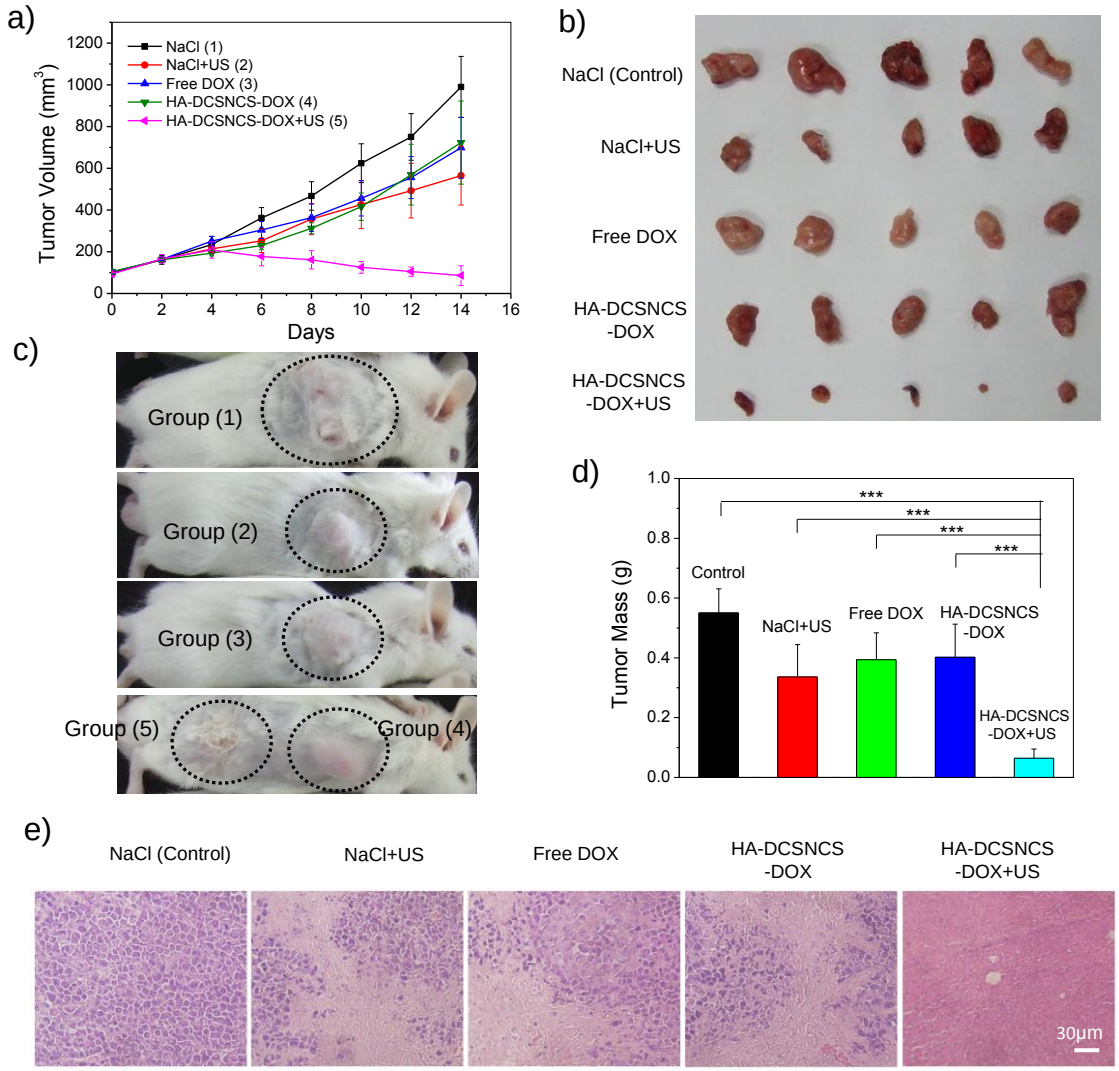

Figure 6. Combined sonodynamic chemotherapy in vivo. a) Tumor growth curves of S180 tumor following the different treatments (5 mice per group). b) Photos of the tumors collected from different groups of mice at the end of treatments (day 14). c) Representative gross photos of mice showing tumors (highlighted by dashed black circles) after different treatments. d) Average weights of tumors at the end of 14 d treatments (***p <0.001, by ANOVA with Tukey's post-test). e) H&E stained images of tumors collected from mice post various treatment.

4. Conclusions

In summary, we have demonstrated a method to construct dual-core@shell nanocomposites comprised of $NaYF_4$, Fe_3O_4 and TiO_2. Several distinct properties including upconversion luminescence, drug loading and magnetic targeted SDT were combined into one simple structure. In vitro experiments, HA-DCSNCs exhibited time dependent cellular uptake and outstanding nucleus targeting effect in KB and MCF-7 cells. Besides good apoptosis induction effect and synergistic anticancer effect were also observed. In vivo experiments, the HA-DCSNCs which synergetically combine chemotherapy with SDT generate better anticancer activity than individual therapy. The novel composite HA-DCSNCs offers an innovative targeting drug delivery platform for multidimensional cancer treatment. It is also expected to combine other kinds of anticancer drugs or sensitizers to generate much more effective treatments for cancer therapy.

Acknowledgements

The work was supported by the National Natural Science Foundation of China (81172999, 81373347) and the Scientific Research Fund of Ministry of Health-Medical Science Major

Technology Fund Project of Zhejiang Province (No. WKJ2012-2-023).

Notes and references

[a] College of Pharmaceutical Sciences, Jiangsu University, Zhenjiang, Jiangsu 212013, China. E-mail: geyanru@ujs.edu.cn
[b] College of Pharmaceutical Sciences, Zhejiang University, Hangzhou, Zhejiang 310058, China. E-mail: jinyizju@hotmail.com
[c] Affiliated Hospital of Jiangsu University, Zhenjiang, Jiangsu 212001, China

† Electronic Supplementary Information (ESI) available: [the size distribution of $NaYF_4$, Fe_3O_4 and DCSNCs, thermogravimetric curves of the DCSNCs and HA-DCSNCs particles, the fluorescence intensity of DOX in various organs, H&E stained images of heart, liver, spleen, lung and kidney.]. See DOI: 10.1039/b000000x/

1 M. Kuroki, K. Hachimine, H. Abe, H. Shibaguchi, S. Maekawa, J. Yanagisawa, T. Kinugasa, T. Tanaka and Y. Yamashita, *Anticancer Res.*, 2007, **27**, 3673-3677.
2 S. Yamaguchi, H. Kobayashi, T. Narita, K. Kanehira, S. Sonezaki, N. Kudo, Y. Kubota, S. Terasaka and K. Houkin, *Ultrason. Sonochem.*, 2011, **18**, 1197-1204.
3 K. Ninomiya, C. Ogino, S. Oshima, S. Sonoke, S. Kuroda and N. Shimizu, *Ultrason. Sonochem.*, 2012, **19**, 607-614.
4 Y. X. Li, P. Wang, P. Zhao, S. J. Zhu, X. B. Wang and Q. H. Liu, *Ultrasonics*, 2012, **52**, 490-496.
5 Z. Ram, Z. R. Cohen, S. Harnof, S. Tal, M. Faibel, D. Nass and S. E. Maier, *Neurosurgery*, 2006, **59**, 949-955.
6 T. Ohmura, T. Fukushima, H. Shibaguchi, S. Yoshizawa, T. Inoue, M. Kuroki, K. Sasaki and S. I. Umemura, *Anticancer Res.*, 2011, **31**, 2527-2533.
7 W. Song, H. D. Cui, R. Zhang, J. H. Zheng and W. W. Cao, *Anticancer Res.*, 2011, **31**, 39-45.
8 H. Abe, M. Kuroki, K. Tachibana, T. L. Li, A. Awasthi, A. Ueno, H. Matsumoto, T. Imakiire, Y. Yamauchi, H. Yamada and A. Ariyoshi, *Anticancer Res.*, 2002, **22**, 1575-1580.
9 J. Xu, Y. Sun, J. J. Huang, C. M. Chen, G. Y. Liu, Y. Jiang, Y. M. Zhao and Z. Y. Jiang, *Bioelectrochemistry*, 2007, **71**, 217-222.
10 Y. Kubota, T. Shuin, C. Kawasaki, M. Hosaka, H. Kitamura, R. Cai, H. Sakai, K. Hashimoto and A. Fujishima, *Brit. J. Cancer*, 1994, **70**, 1107.
11 E. A. Rozhkova, I. Ulasov, B. Lai, N. M. Dimitrijevic, M. S. Lesniak and T. Rajh, *Nano Lett.*, 2009, **9**, 3337-3342.
12 Y. Y. Song, F. Schmidt-Stein, S. Bauer and P. Schmuki, *J. Am. Chem. Soc.*, 2009, **131**, 4230-4232.
13 D. K. Chatterjee, M. K. Gnanasammandhan and Y. Zhang, *Small*, 2010, **6**, 2781-2795.
14 F. Wang and X. G. Liu, *J. Am. Chem. Soc.*, 2008, **130**, 5642-5643.
15 L. Cheng, K. Yang, Y. G. Li, J. H. Chen, C. Wang, M. W. Shao, S. T. Lee and Z. Liu, *Angew. Chem. Int. Ed.*, 2011, **50**, 7385-7390.
16 G. S. Hong, J. T. Robinson, Y. J. Zhang, S. Diao, A. L. Antaris, Q. B. Wang and H. J. Dai, *Angew. Chem. Int. Ed.*, 2012, **51**, 9818-9821.
17 Y. P. Gu, R. Cui, Z. L. Zhang, Z. X. Xie and D. W. Pang, *J. Am. Chem. Soc.*, 2012, **134**, 79-82.
18 M. B. Zheng, C. X. Yue, Y. F. Ma, P. Gong, P. F. Zhao, C. F. Zheng, Z. H. Sheng, P. F. Zhang, Z. H. Wang and L. T. Cai, *Acs Nano*, 2013, **7**, 2056-2067.
19 L. Cheng, K. Yang, Q. Chen and Z. Liu, *Acs Nano*, 2012, **6**, 5605-5613.
20 Z. Q. Li, Y. Zhang and S. Jiang, *Adv. Mater.*, 2008, **20**, 4765-4769.
21 G. Tian, Z. J. Gu, L. J. Zhou, W. Y. Yin, X. X. Liu, L. Yan, S. Jin, W. L. Ren, G. M. Xing, S. J. Li and Y. L. Zhao, *Adv. Mater.*, 2012, **24**, 1226-1231.
22 M. Haase and H. Schafer, *Angew. Chem. Int. Ed.*, 2011, **50**, 5808-5829.
23 F. Zhang, G. B. Braun, A. Pallaoro, Y. C. Zhang, Y. F. Shi, D. X. Cui, M. Moskovits, D. Y. Zhao and G. D. Stucky, *Nano Lett.*, 2012, **12**, 61-67.
24 X. J. Zhu, J. Zhou, M. Chen, M. Shi, W. Feng and F. Y. Li, *Biomaterials*, 2012, **33**, 4618-4627.
25 L. Cheng, K. Yang, Y. G. Li, X. Zeng, M. W. Shao, S. T. Lee and Z. Liu, *Biomaterials*, 2012, **33**, 2215-2222.
26 J. Liu, Z. K. Sun, Y. H. Deng, Y. Zou, C. Y. Li, X. H. Guo, L. Q. Xiong, Y. Gao, F. Y. Li and D. Y. Zhao, *Angew. Chem. Int. Ed.*, 2009, **48**, 5875-5879.
27 S. Shen, F. Kong, X. Guo, L. Wu, H. Shen, M. Xie, X. Wang, Y. Jin and Y. Ge, *Nanoscale*, 2013, 5, 8056–8066.
28 D. Pasqui, L. Golini, C. Della Giovampaola, A. Atrei and R. Barbucci, *Biomacromolecules*, 2011, **12**, 1243-1249.
29 W. F. Ma, Y. Zhang, L. L. Li, L. J. You, P. Zhang, Y. T. Zhang, J. M. Li, M. Yu, J. Guo, H. J. Lu and C. C. Wang, *Acs Nano*, 2012, **6**, 3179-3188.
30 W. Li, J. Yang, Z. Wu, J. Wang, B. Li, S. Feng, Y. Deng , F. Zhang and D. Zhao. *J Am Chem Soc.* 2012, **134**,11864-11867.
31 Z. Liu, X. M. Sun, N. Nakayama-Ratchford and H. J. Dai, *Acs Nano*, 2007, **1**, 50-56.
32 J. You, G. D. Zhang and C. Li, *Acs Nano*, 2010, **4**, 1033-1041.
33 C. J. Yu, S. M. Wu and W. L. Tseng, *Anal. Chem.*, 2013, **85**, 8559−8565
34 A. S. Al-Kady, M. Gaber, M. M. Hussein and E.-Z. M. Ebeid, *Spectrochim. Acta, Part A*, 2011, **83**, 398–405
35 W. Tang, Q. H. Liu, X. B. Wang, P. Wang, J. Zhang and B. Cao, *Ultrasonics*, 2009, **49**, 786-793.
36 H. Mizutani, S. Tada-Oikawa, Y. Hiraku, M. Kojima and S. Kawanishi, *Life Sci.*, 2005, **76**, 1439-1453.
37 T. Fernandez Cabada, C. Sanchez Lopez de Pablo, A. Martinez Serrano, F. del Pozo Guerrero, J. J. Serrano Olmedo and M. Ramos Gomez, *Int. J. Nanomed.*, 2012, **7**, 1511-1523.

Journal of Materials Chemistry B RSCPublishing

ARTICLE

Table of contents

Dual-core@shell-structured Fe_3O_4-$NaYF_4$@TiO_2 Nanocomposites as Magnetic Targeting Drug Carrier for Bioimaging and Combined Chemo-sonodynamic Therapy